

**Raman backscattering and amplification in a gas jet plasma**

Y. Ping, I. Geltner, and S. Suckewer

*Princeton University, Princeton, New Jersey 08544*

(Received 30 July 2002; published 6 January 2003)

Raman backscattering (RBS) of a picosecond 800-nm laser pulse from a gas jet plasma has been observed. The frequency shifts are in agreement with independent interferometric density measurements and the band width of the RBS is consistent with the linear growth rate. Raman amplification of a subpicosecond seed pulse, provided by an optical parametric oscillator and tuned to the spectral range of the RBS, has been obtained. The Raman resonance is confirmed by simultaneous plasma density measurements.

DOI: 10.1103/PhysRevE.67.016401

PACS number(s): 52.38.-r, 42.65.Dr, 52.50.Jm

**I. INTRODUCTION**

Raman backscattering (RBS) in plasma is a three-wave process, in which an electromagnetic wave decays into a Langmuir wave and a redshifted backward electromagnetic wave. Since its first observation from laser-plasma interaction [1], there has been extensive studies of this instability, not only the phenomenon itself but also its usefulness in laser-plasma physics. For example, measuring the frequency shift of the backscattered light has become a very useful diagnostic of plasma density [2,3] since the frequency difference between the incident and the backscattered waves is equal to the plasma frequency  $\omega_p$ , which is proportional to  $n_e^{1/2}$ .

Other important applications include using the Raman instability as a means to compress laser pulses. This scheme was initialized by the observation of intense light bursts in stimulated RBS from carbon disulfide, which had a peak power one order of magnitude higher than the incident pump power [4]. The compression of laser pulses is achieved by the sharpening of the wave front since the tail part interacts with a depleted pump and is not pumped as strongly as the front. Early work on the compression of laser pulses was carried out in gases, where molecular vibrations serve as the Raman scatterers [5]. Raman compression of KrF laser pulses (248 nm) from 20 ns to 30 ps with an energy efficiency of 22% was reported, resulting in a power gain of 150 [6,7]. Generation of picosecond pulses in the infrared regime by two-stage compression of an 8-ns laser pulse was also achieved in gases [8]. A Raman compressor with plasma as the medium was proposed by Capjack *et al.* [9] in order to avoid the troublesome backward second-Stokes wave which limits the efficiency and compression ratio in gas compressors. Another advantage of the plasma medium is that plasma can handle ultrahigh laser power whereas the maximum laser power in gases is limited by ionization.

When seeded by a frequency-matched laser pulse, the Raman compressor can also serve as an amplifier. Energy transfer between two nanosecond laser pulses, mediated by an ion acoustic wave [10] or a Langmuir wave [11], has been observed. Early studies have recognized the difficulties of ultrashort pulse compression in plasma because of the relatively narrow band width of Raman amplification, which is a characteristic of the linear regime. Recently, new effects were identified in the nonlinear behavior of plasma when

interacting with ultraintense laser pulses [12–14]. Theoretical studies have shown that the amplified pulse duration decreases inversely proportional to the pulse amplitude and compression from picosecond to femtosecond is achievable in the nonlinear regime [15]. Raman amplification in combination with the compression effect in plasma can potentially overcome the power limit of current chirped-pulse-amplification laser systems, which is set by the thermal damage threshold of the optics.

In our recent papers [16,17] we have presented, to the best of our knowledge, the first experimental results on ultrashort pulse amplification in microcapillary plasma by a counter-propagating pumping pulse, where an amplification of up to 8 has been obtained. However, the microcapillary plasma is quite difficult to diagnose due to poor access to the plasma [18], and the longitudinal uniformity is difficult to control. In contrast, a high pressure gas jet can provide a quite uniform plasma column suitable for Raman amplification, and it is an open system, allowing for simultaneous plasma density measurements. Furthermore, as was demonstrated earlier [19,20], good guiding of laser pulses is possible in such a gas jet. Therefore, we have concentrated our effort on studies of Raman backscattering and amplification in a gas jet plasma, which is the subject of the present paper.

The experiments were carried out in two steps. First, the RBS of a 170-ps laser pulse at 800 nm (the pumping pulse) was observed in the gas jet plasma. The plasma density calculated from the frequency shift was compared with the interferometric measurements. Second, the wavelength of the output pulses (the seed pulse) from an optical parametric oscillator (OPO) was tuned to the regime of the RBS wavelengths in order to match the plasma density. The pump and the seed pulses propagated in the gas jet plasma in the opposite directions, and the Raman amplification was characterized by the ratio between the amplified pulse spectrum and a reference spectrum. The Raman resonance peak in the spectrum was consistent with the simultaneous plasma density measurement.

**II. OBSERVATION OF RAMAN BACKSCATTERING**

The schematic of the experimental setup for the observation of RBS is presented in Fig. 1. The gas jet, with an orifice of  $1 \times 6$  mm, was located in a vacuum chamber. The plasma was created through optical breakdown in the gas jet by an

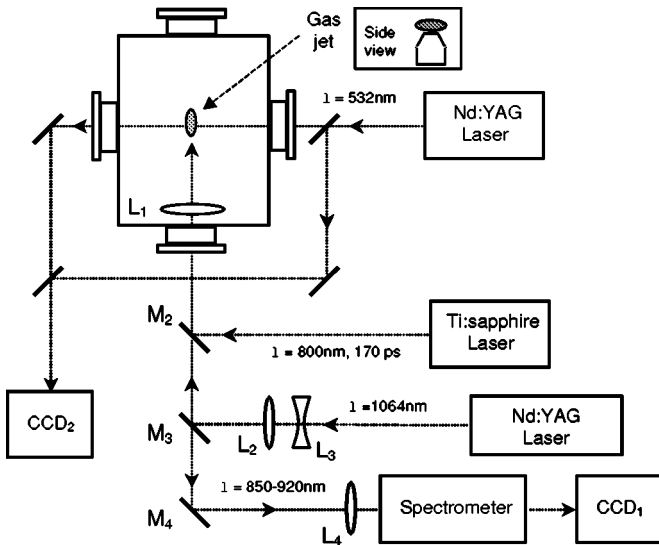


FIG. 1. Experimental setup for observation of RBS in the high-pressure gas jet plasma.

additional laser pulse at 1064 nm (prepulse, up to 400 mJ in 7 ns). A telescope consisting of two lenses  $L_2$  and  $L_3$  was used to adjust the focal position of the prepulse in the gas jet. The output pulse from the 800-nm laser system (pumping pulse, up to 300 mJ in 170 ps) was focused by an F/10 lens  $L_1$  into the gas jet plasma to generate Raman backscattering. The backscattered light, collected by  $L_1$ , passed through two mirrors  $M_2$  and  $M_3$  and was focused into a spectrometer. The spectrum was displayed by a charge-coupled-device camera (CCD<sub>1</sub>). The observable wavelength range was 850–920 nm, limited by the reflection band width of  $M_2$  and  $M_3$ . An interferometer was set up from the side to measure the plasma density distribution. The interferogram was monitored by another camera (CCD<sub>2</sub>). To minimize the variation of the plasma density through additional ionization by the pumping pulse, propane ( $C_3H_8$ ), which has a high concentration of H, was chosen as the injected gas.

A typical interferogram of the gas jet plasma is shown in Fig. 2(a). The energies of the 7-ns prepulse and the 800-nm 170-ps pumping pulse were both about 200 mJ and the delay between them was 60 ns. The plasma column at this delay is about 300  $\mu\text{m}$  wide and 1 mm long. The plasma density along the axis is plotted in Fig. 2(b), showing that the density was  $\sim 2 \times 10^{19} \text{ cm}^{-3}$  and the distribution along the axis was quite uniform, which is important for the Raman amplification experiment.

Typical spectra of the RBS at various delays are shown in Figs. 3(b)–3(d), together with the spectrum of the incident pumping pulse for comparison [Fig. 3(a)]. From 60 ns to 100 ns the central wavelength of the RBS shifts from 906 nm to 889 nm, corresponding to a plasma density decrease from 2.4 to  $1.7 \times 10^{19} \text{ cm}^{-3}$ . The band width of the RBS varies from shot to shot, mostly being 3 nm [full width at half maximum, Fig. 3(b) and 3(d)] and occasionally reaching 8 nm [Fig. 3(c)], which is narrower than that of the pumping pulse (11 nm). At low intensities the band width of the RBS is equal to twice the linear growth rate [21],  $\gamma_{RBS} = a_1(\omega_1 \omega_p/4)^{1/2}$ , where  $\omega_1$  is the frequency of the pumping pulse and  $a_1$

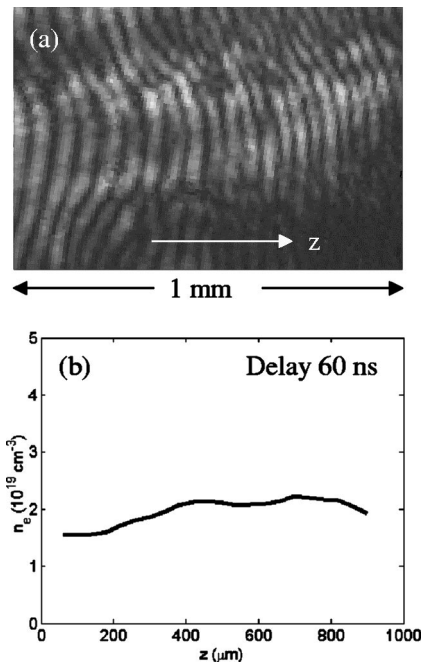


FIG. 2. (a) An interferogram taken at a delay of 60 ns. (b) Plasma density distribution along the axis, calculated from (a) and averaged over a central area of 40  $\mu\text{m}$ . The energies of the prepulse and the 800 nm pulse are both 200 mJ.

$= 0.85 \times 10^{-9} \lambda_1 I_1^{1/2}$  is its normalized vector potential (the pump wavelength  $\lambda_1$  is in  $\mu\text{m}$  and the intensity  $I_1$  is in  $\text{W}/\text{cm}^2$ ). In our case,  $\gamma_{RBS}$  is estimated to be  $\sim 2.8 \times 10^{12} \text{ s}^{-1}$  for  $I_1 \approx 1.2 \times 10^{14} \text{ W}/\text{cm}^2$ ,  $\lambda_1 = 800 \text{ nm}$  and  $n_e \approx 2 \times 10^{19} \text{ cm}^{-3}$ , which corresponds to a band width of 2.5 nm at 900 nm. This agrees well with experimental measurements ( $\sim 3 \text{ nm}$ ). The occasionally larger band width (8 nm) is probably due to plasma density gradients that broaden the resonance. Such a spectral band width (3–8 nm) corresponds to a transform-limited pulse duration of 250–600 fs.

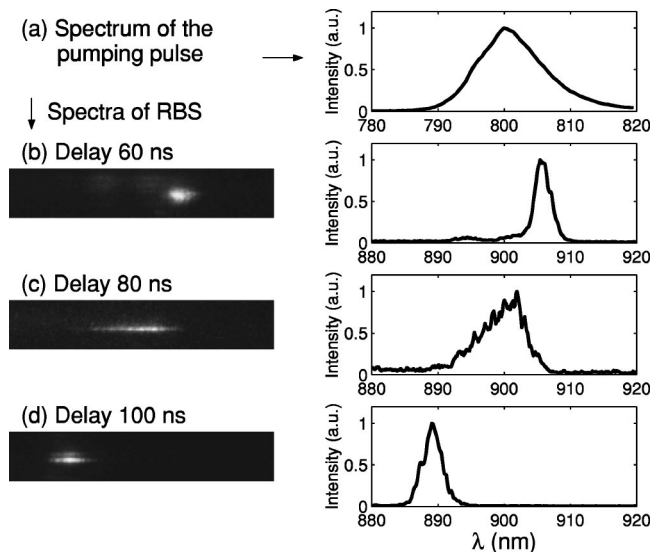


FIG. 3. (a) Spectrum of the pumping pulse. (b)–(d) Spectra of RBS at three delays.

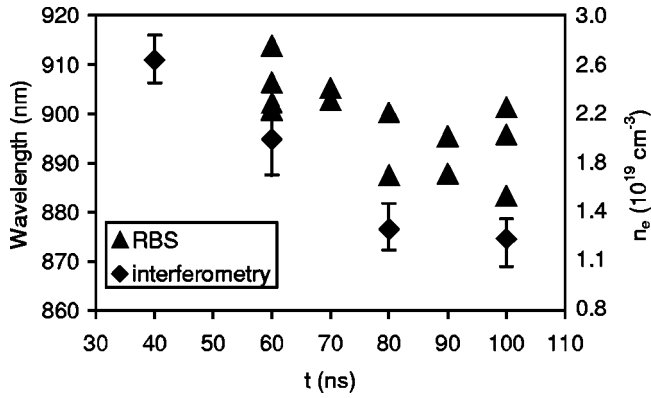


FIG. 4. Wavelengths of RBS (triangles) and the measured plasma density (diamonds) as a function of delay.

The plasma density measured by the interferometer (averaged along the axis) vs delay is shown in Fig. 4 (diamonds), indicating that the density decreases from  $2.7$  to  $1.3 \times 10^{19} \text{ cm}^{-3}$  as the delay increases from  $40$  ns to  $100$  ns. The wavelengths of the RBS are also shown in Fig. 3 (triangles), exhibiting a similar trend as a function of the delay. The plasma density calculated from the frequency shift is generally higher than the interferometric measurements, and the difference becomes larger at longer delays. For instance, the average density obtained from the frequency shift at  $60$  ns is  $2.3 \times 10^{19} \text{ cm}^{-3}$ ,  $15\%$  higher than the interferometric measurement ( $2.0 \times 10^{19} \text{ cm}^{-3}$ ), while at  $100$  ns the former is  $1.9 \times 10^{19} \text{ cm}^{-3}$ , about  $50\%$  higher than the latter ( $1.3 \times 10^{19} \text{ cm}^{-3}$ ). We believe that this is due to additional ionization induced by the powerful pumping pulse. The plasma created by the prepulse is not fully ionized and the incidence of the pumping pulse leads to a slightly higher  $n_e$ . As the delay increases, the plasma cools down and recombines. Therefore, more neutrals or low-ionization-stage ions are available to be ionized. As a result, the effect of additional ionization becomes more significant at longer delays, leading to the increased difference between the two data sets. Since the focal spot of the  $800$  nm pulse ( $\sim 30 \mu\text{m}$ ) is much smaller than the width of the plasma column, the local enhancement of the plasma density can hardly be detected by the interferometer as the phase shift in the interferometry is integrated in the transverse direction over the whole width of the plasma column ( $\sim 300 \mu\text{m}$ ).

### III. RAMAN AMPLIFICATION IN THE GAS JET PLASMA

In order to investigate Raman amplification an ultrashort laser pulse at a proper wavelength is required to serve as the seed pulse. It has been demonstrated that the output pulses from an OPO are suitable for this task [17]. The wavelength tunability of the OPO also provided us with the freedom for matching the plasma density. The physics of the optical parametric conversion is quite similar to that of the harmonic generation in nonlinear crystals but the process goes in the opposite direction: one high-energy photon is “split” into two lower-energy photons in the parametric conversion, one is called the signal and the other is the idler,  $\omega_{\text{pump}} \rightarrow \omega_{\text{signal}} + \omega_{\text{idler}}$ . The wavelengths of the signal and the

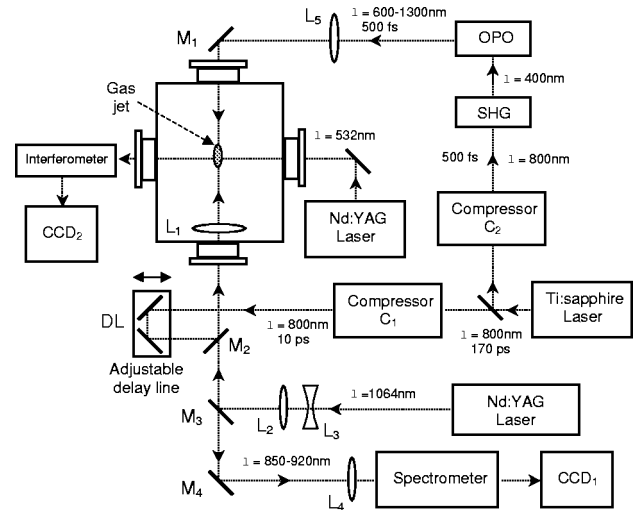


FIG. 5. Experimental setup for Raman amplification in the gas jet plasma.

idler can be varied by adjusting the phase-matching angle of the crystal. The tuning range of an OPO pumped at  $400$  nm is  $\approx 600\text{--}1300$  nm [22].

The other change in the experimental setup is related to the pumping pulse. The energy of the observed RBS generated by the  $800$  nm,  $170$  ps pulse was much higher than that of the seed pulse from the OPO. If the  $170$  ps pulse had been used as the pump for the Raman amplification experiment, the spontaneous RBS would have totally dominated over the amplified short seed pulse because the RBS would have had much more time to grow. To avoid such a problem the  $800$ -nm pulse was compressed down to  $10$  ps so that the energy of the spontaneous RBS was significantly reduced while keeping the same pumping intensity. The schematic of the experimental setup for Raman amplification in the high-pressure gas jet plasma is shown in Fig. 5.

The  $800$ -nm laser pulse was split into two parts: one ( $95\%$  of the total energy) passed through compressor  $C_1$  and was compressed to  $\sim 10$  ps to serve as the pumping pulse; the other ( $5\%$  of the total energy) was compressed by another compressor,  $C_2$ , to  $\sim 500$  fs and was frequency doubled by a SHG crystal to pump an OPO and generate the seed pulse. After being reflected by mirror  $M_1$ , passing through the gas jet and two mirrors  $M_2$  and  $M_3$ , the wavelength range of the seed pulse narrowed down to  $850\text{--}920$  nm, as explained in the preceding section, covering a density range from  $1$  to  $3 \times 10^{19} \text{ cm}^{-3}$ . Similar to the arrangement in the microcapillary experiment [17], a small portion of the seed pulse was split out and sent to the spectrometer directly, providing a reference spectrum. The orifice of the gas injector was  $1$  mm in diameter, which limited the length of the high density plasma (across the orifice) to below  $1$  mm.

One of the obstacles encountered in our previous experiment in microcapillaries [16,17] is that there was strong inverse Bremsstrahlung (IB) absorption of the laser pulses due to the high density ( $1\text{--}3 \times 10^{20} \text{ cm}^{-3}$ ) and low temperature ( $\sim 20$  eV). With the new pair of laser wavelengths the matching density is reduced to  $10^{19} \text{ cm}^{-3}$ , resulting in a de-

crease in the IB by more than two orders of magnitude. Although the temperature in the gas jet plasma ( $\sim 5$  eV) was lower than in the microcapillary plasma [18], the estimated IB damping length is  $\sim 1$  cm, much longer than in the microcapillary experiment. Such IB absorption is negligible for the 0.5-mm-long plasma used in this experiment.

Since the pumping pulse was only 10 ps long, the paths of the seed and the pump pulses (each traveling more than 10 m from the laser system to the chamber) had to be matched with an accuracy better than 3 mm to ensure the temporal overlap of the two pulses. The high precision synchronization between the seed and the pumping pulses was accomplished by using a noncollinear autocorrelator setup in the vacuum chamber. (This type of second-harmonic autocorrelation is a standard technique for subpicosecond duration measurements [23].) During the experiment the delay line of the pumping pulse was also scanned over a sufficiently large distance to ensure that the “synchronization point” was well covered.

With the 10-ps pumping pulse the spontaneous RBS became observable only when the energy of the pumping pulse exceeded 50 mJ. The observation of Raman amplification was carried out in two ways. One was to find the resonance peaks in the seed pulse spectrum while keeping the pumping energy below the threshold for spontaneous RBS. In such a case the procedure of amplification measurement was the same as in the earlier experiments in microcapillaries [17]. The amplification was characterized by the ratio of the amplified seed pulse spectrum to the reference spectrum,  $S_p/S_0$ . The second way was to investigate the effect of the seed pulse on the amplitude of the RBS. This effect was characterized by the ratio of the energies of the seeded RBS,  $S_{sd}$ , to the spontaneous RBS,  $S_{sp}$ .

The ratio of  $S_p/S_0$  at various relative delays between the 500-fs seed pulse and the 10-ps pumping pulse was measured. The energy of the pump was 40 mJ, which was below the RBS threshold. At the optimum delay there was a resonance peak in the spectrum, with an amplification ratio of  $\sim 2$ , as shown in Fig. 6(a). When the two pulses were off in time the ratio was close to 1 in the whole spectral range. In Fig. 6(b) is shown the simultaneously measured plasma density distribution along the axis by the interferometer at the optimum delay. The horizontal coordinate in Fig. 6(a) has been converted to the corresponding density in order to compare with the density measurement. The plasma length, for which the density was in the appropriate range of  $1.1$ – $1.5 \times 10^{19}$  cm $^{-3}$ , was  $\sim 0.5$  mm. The resonance density in Fig. 6(a) agrees well with the interferometrically measured density. Since there were strong plasma density gradients along the axis the resonance peak was relatively broad, spreading from  $1.1$  to  $1.4 \times 10^{19}$  cm $^{-3}$  (870–880 nm).

When the pump energy was increased to 60 mJ and significant spontaneous RBS was observed, the ratio of  $S_{sd}/S_{sp}$  as a function of the relative delay was measured. The RBS was enhanced by a factor of  $\sim 1.5$  at the same relative delay as the resonance peak was observed. We should emphasize that the actual amplification was larger than just the simple ratio of  $S_{sd}/S_{sp}$ , because of the difference in the spontaneous scattering and the amplification time. The growing time

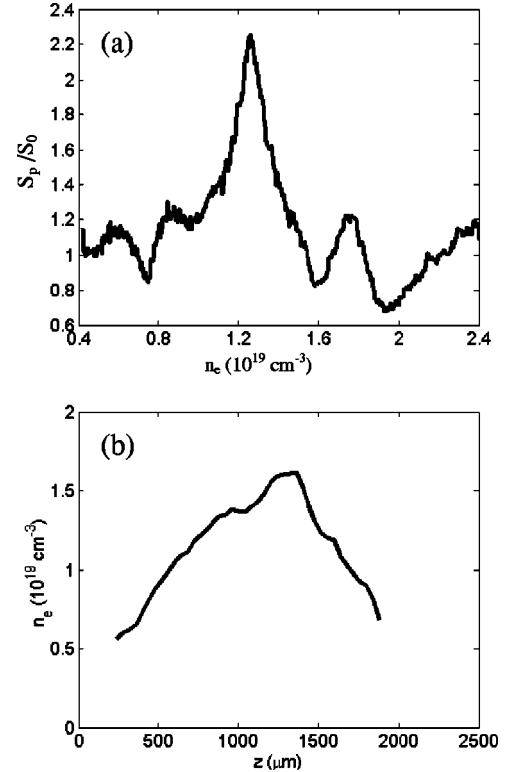


FIG. 6. (a) Ratio of  $S_p/S_0$  at the optimum relative delay for Raman amplification. (b) Plasma density distribution along the axis measured simultaneously by the interferometer.

for the spontaneous RBS was 10 ps (the pulse duration of the pumping pulse), while the amplification time for the seed pulse was about 3 ps ( $2L_p/c$ , for a plasma length  $L_p \sim 0.5$  mm). Due to the unstable nature of RBS the fluctuations in the amplitude of the backscattered radiation were very large. The fluctuations could be suppressed if the seed pulse would be much more intense than the spontaneous RBS and a significant depletion of the pump would take place.

The density gradient along the axis is one critical factor limiting the amplification. As presented in Sec. II, the relative band width of RBS is  $\Delta\omega_2/\omega_2 \sim 2\gamma_{RBS}/\omega_2 \approx 0.003$  ( $\omega_2$  is the frequency of the backscattered light). The corresponding density variation is  $\Delta n_e/n_e = 2\Delta\omega_p/\omega_p = 2\Delta\omega_2/(\omega_1 - \omega_2) \sim 0.06$ . This means that if the density perturbation exceeds 6% the interaction will be out of resonance (for a single-frequency pump). From the measured density distribution, a density variation of 6% corresponds to a spatial scale of  $\Delta z \sim 60$   $\mu$ m. Given the linear growth rate,  $\gamma_{RBS} \approx 2.3 \times 10^{12}$  s $^{-1}$  for  $n_e \approx 1 \times 10^{19}$  cm $^{-3}$ , the theoretical predicted amplification for such a short plasma length is  $\exp(2\gamma_{RBS}\Delta z/c) \approx 2.5$ , agreeing very well with the measurements.

#### IV. CONCLUSION AND DISCUSSION

In conclusion, we have shown Raman backscattering and amplification in a gas jet plasma. The frequency shifts of the

RBS agree well with independent interferometric density measurements. The band width of the RBS is limited to twice of the linear growth rate and is sometimes broadened by plasma density gradients. Amplification of a 500-fs counterpropagating seed pulse by a factor of 2 has been observed. The Raman resonance is confirmed by simultaneous plasma density measurements.

Compared to our previous experiments in microcapillaries, there are two major improvements in the experimental setup. First, by replacing the microcapillary plasma by a high-pressure gas jet plasma, it allows for simultaneous plasma density measurements so that the Raman resonance can be confirmed. In the microcapillary case the plasma is created by laser ablation of the capillary wall. The reproducibility is sensitive to the alignment of the laser pulse and the wall condition, which are difficult to control [18]. In contrast, the gas jet plasma provides much better reproducibility with fresh gas used for each shot. The second improvement is related to lower plasma density. By employing a new pair of laser wavelengths, the matching density is decreased by more than an order of magnitude and the inverse Bremsstrahlung absorption, which is proportional to  $n_e^2$ , is reduced by two orders of magnitude. Therefore, the strong damping of the laser pulses encountered in the microcapillary experiment is significantly reduced.

The observed Raman amplification in the gas jet plasma was modest ( $\sim 2$ ) due to the short plasma length (related to uniformity) and the modest pumping intensity. As analyzed at the end of Sec. III, the uniformity of the plasma density is critical for the amplification in the linear regime due to the narrow band width of the gain. By employing a line-focus axicon instead of a point-focus spherical lens the gas jet plasma can be improved to be longer and more uniform [19]. On the other hand, since the band width is twice of the growth rate  $\gamma_{RBS}$ , which is proportional to the square root of the pumping intensity  $I_1$ , an increase in  $I_1$  can broaden the gain band width, thus relieving the strict requirement on the uniformity of the plasma density. For the pumping intensity used in the present experiment,  $I_1 \sim 1 \times 10^{14}$  W/cm<sup>2</sup>, the maximum density variation is 6%, while for  $I_1 \sim 1$

$\times 10^{15}$  W/cm<sup>2</sup>, the density tolerance can be 20%, which is already a reasonable requirement for experiments. Therefore, increasing the pumping intensity has a twofold benefit: to obtain larger amplification and to lessen experimental difficulties. In the present experiment we did not use pumping intensities above  $10^{14}$  W/cm<sup>2</sup> for the amplification because of the appearance of spontaneous RBS. The seed pulse produced by the OPO was too weak to deplete the pump. Therefore, the spontaneous RBS has more time to grow and it dominates over the amplified pulse. A higher-intensity seed pulse is desired in order to suppress the spontaneous RBS and to explore Raman amplification in the nonlinear regime. A detuning scheme has been proposed to overcome the instabilities of the pumping pulse by an appropriate combination of density gradient and pump chirping [24].

Further investigations will include enhancing the efficiency of the OPO for the generation of higher-energy seed pulses, improving the gas jet and the optical system to make longer and more uniform plasma. Another factor affecting the uniformity and the interaction length is the additional ionization by the pumping pulse, as indicated by comparing the wavelength shifts of the RBS and the interferometric plasma density measurements (Sec. II, Fig. 4). The additional ionization can result in the defocusing of the pumping pulse, limiting both the interaction length and the pumping intensity. To eliminate the ionization defocusing effect the plasma should be fully ionized, or at least have the next level too high for the pumping pulse to ionize. Furthermore, as the interaction length becomes longer, the diffraction of the laser pulses will be the limiting factor and waveguiding will be necessary to extend the interaction beyond the Rayleigh length.

#### ACKNOWLEDGMENTS

We would like to thank Dr. A. Morozov for his help in the experiments, and Professor N. J. Fisch for stimulating discussions. We would also like to thank N. Tkach for technical support. This work was supported by DARPA and NSF (PHYS) grants.

- 
- [1] R.G. Watt, R.D. Brooks, and Z.A. Pietrzyk, *Phys. Rev. Lett.* **41**, 170 (1978).
  - [2] M.D. Perry, C. Darrow, C. Coverdale, and J.K. Crane, *Opt. Lett.* **17**, 523 (1992).
  - [3] T.G. Jones, K. Krushelnick, A. Ting, D. Kaganovich, C.I. Moore, and A. Morozov, *Rev. Sci. Instrum.* **73**, 2259 (2002).
  - [4] M. Maier, W. Kaiser, and J. Giordmaine, *Phys. Rev. Lett.* **17**, 1275 (1966).
  - [5] J.R. Murray, J. Goldhar, D. Eimerl, and A. Szoke, *IEEE J. Quantum Electron.* **15**, 342 (1979).
  - [6] H. Nishioka, K. Kimura, K. Ueda, and H. Takuma, *IEEE J. Quantum Electron.* **29**, 2251 (1993).
  - [7] E. Takahashi, Y. Matsumoto, I. Matsushima, I. Okuda, Y. Owadano, and K. Kuwahara, *Fusion Eng. Des.* **44**, 133 (1999).
  - [8] V.V. Akulinichev, V.A. Gorbunov, and E.G. Pivinskii, *Quantum Electron.* **27**, 351 (1997).
  - [9] C.E. Capjack, C.R. James, and J.N. McMullin, *J. Appl. Phys.* **53**, 4046 (1982).
  - [10] R.K. Kirkwood *et al.*, *Phys. Rev. Lett.* **76**, 2065 (1996).
  - [11] R.K. Kirkwood *et al.*, *Phys. Rev. Lett.* **83**, 2965 (1999).
  - [12] G. Shvets, N.J. Fisch, A. Pukhov, and J.M. ter Vehn, *Phys. Rev. Lett.* **81**, 4879 (1998).
  - [13] V.M. Malkin, G. Shvets, and N.J. Fisch, *Phys. Rev. Lett.* **82**, 4448 (1999).
  - [14] V.M. Malkin and N.J. Fisch, *Phys. Plasmas* **8**, 4698 (2001).
  - [15] V.M. Malkin, G. Shvets, and N.J. Fisch, *Phys. Plasmas* **7**, 2232 (2000).
  - [16] Y. Ping, I. Geltner, N.J. Fisch, G. Shvets, and S. Suckewer, *Phys. Rev. E* **62**, R4532 (2000).
  - [17] Y. Ping, I. Geltner, A. Morozov, N. J. Fisch, and S. Suckewer, *Phys. Rev. E* **66**, 046401 (2002).

- [18] Y. Ping, I. Geltner, A. Morozov, and S. Suckewer, *Phys. Plasmas* **9**, 4756 (2002).
- [19] C.G. Durfee, J. Lynch, and H.M. Milchberg, *Phys. Rev. E* **51**, 2368 (1995).
- [20] A. Morozov, Y. Ping, S. Suckewer, A. Bartnik, and H. Fiedorowicz, *Proc. SPIE* **3156**, 214 (1997).
- [21] C.B. Darrow, C. Coverdale, M.D. Perry, W.B. Mori, C. Clayton, K. Marsh, and C. Joshi, *Phys. Rev. Lett.* **69**, 442 (1992).
- [22] M.K. Reed, M.K. Steinershepard, M.S. Armas, and D.K. Negus, *J. Opt. Soc. Am. B* **12**, 2229 (1995).
- [23] C. Kolmeder, W. Zinth, and W. Kaiser, *Opt. Commun.* **30**, 453 (1979).
- [24] V.M. Malkin, G. Shvets, and N.J. Fisch, *Phys. Rev. Lett.* **84**, 1208 (2000).